INSTITUTE OF PHYSICS PUBLISHING JOURNAL OF PHYSICS D: APPLIED PHYSICS

J. Phys. D: Appl. Phys. **34** (2001) 624–630 www.iop.org/Journals/jd PII: S0022-3727(01)19047-9

Influence of the Stark effect on the fluorescence polarization of $X\,^1\Sigma \rightarrow B\,^1\Pi$-state laser-excited NaRb: application to the direct imaging of electric fields

Marcis Auzinsh, Ruvin Ferber, Olga Nikolayeva, Neil Shafer-Ray and Maris Tamanis

The University of Latvia, 19 Rainis Boulevard, Latvia–1586

Received 15 November 2000

Abstract

We investigate the possibility of using the electric-field-dependent laser-induced fluorescence scheme $X\,^1\Sigma(v'', J'') \rightarrow B\,^1\Pi(v', J') \rightarrow X\,^1\Sigma(v, J = J', J' \pm 1)$ to create an image (or movie) of the electric field surrounding an object. Specifically we find that when NaRb is probed in this way, vector correlations between the excitation laser polarization, fluorescence radiation polarization, and electric field vector are sensitive to the magnitude of the electric field, even when the wavelength of the fluorescence (and hence final state J) is not resolved.

1. Introduction

The importance of plasmas to material processing has inspired experimental studies of the complex flow of glow discharges. Of particular importance has been a host of techniques developed to measure the spatial dependence of the electric field in the plasma. Among the most successful of these are optical techniques that take advantage of changes in the spectra of atoms and molecules caused by electric fields (the Stark effect). These optical techniques are reviewed by Lawler and Doughty [1]. One of the most successful schemes for field measurement, first demonstrated by Moore *et al* [2], takes advantage of the field-induced breakdown of parity selection rules in the laser-induced fluorescence between $^1\Sigma$ and $^1\Pi$ states of diatomic molecules. In the absence of an electric field, dipole selection rules require that the laser-induced $^1\Sigma(v'', J'') \rightarrow {}^1\Pi(v', J')$ transition occurs only to the Λ-doublet component of the $^1\Pi(v', J')$ state that has opposite total parity as the ground $^1\Sigma(v'', J'')$ state. The field-free fluorescence signal must again change parity as the $^1\Pi(v', J')$ fluoresces to the $^1\Sigma(v, J)$ state. For this reason, the parity of the initial $^1\Sigma(v'', J'')$ state must match the parity of the final $X\,^1\Sigma(v, J)$ state. This fact implies that, in the absence of an electric field, if one induces the Q-branch transition $^1\Sigma(v'', J') \rightarrow {}^1\Pi(v', J')$, only Q-branch transitions $^1\Pi(v', J') \rightarrow {}^1\Sigma(v, J')$ contribute to the fluorescence. If instead an R- or P-branch transition $^1\Sigma(v'', J' \pm 1) \rightarrow {}^1\Pi(v', J')$ is induced, only R- and P-branch fluorescence $^1\Pi(v', J') \rightarrow {}^1\Sigma(v, J' \pm 1)$ is observed. In the presence of a field, however, parity is no longer a good quantum number and these selection rules break down. Thus the ratio of Q-branch fluorescence to R- and P-branch fluorescence is sensitive to the local electric field. This technique was first demonstrated by Moore and coworkers using BCl [2]. The field-measurement technique has since been adapted to NaK [3, 4]. A complete theory of polarization-and-field-dependent fluorescence has been presented by Derouard and Alexander [5] and, more recently, by our group [6].

In the NaK studies, spectacular field-dependence polarization effects are observed [3, 4]. The fact that the polarization-dependent fluorescence intensity depends strongly on the electric field suggests an improved field-imaging scheme. In this scheme, it is no longer necessary to spectroscopically resolve the Q-branch fluorescence from the R- and P-branch fluorescence. Instead the fluorescence is filtered from scattered laser light and then measured at specific polarizations with a CCD camera (figure 1). The elimination of the need to resolve the wavelength of the fluorescence may prove to be advantageous: instead of the time-consuming process of creating a rastered image, the technique presented here could use a single physical setup to create a photographic image (or video) of the electric field surrounding an object.

0022-3727/01/040624+07$30.00

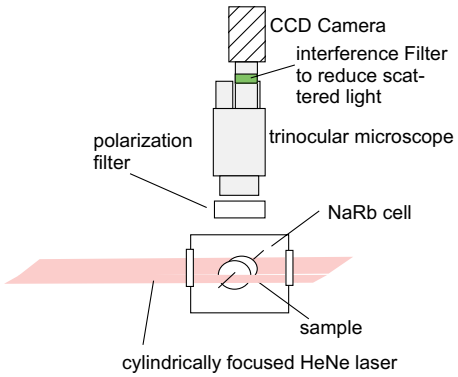

Figure 1. Proposed configuration for imaging the electric field in a plasma.

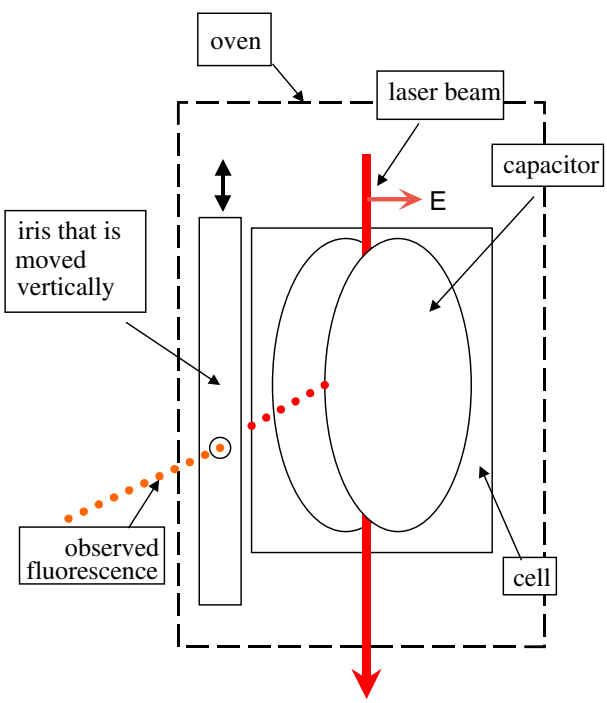

Figure 2. Schematic diagram of the experimental setup.

Here we present both experimental and theoretical evidence that such an electric-field camera is feasible.

Experimental data are gathered using equipment on hand in our laboratory. Because the X $^1\Sigma(v'' = 10, J' = 24) \rightarrow$ B $^1\Pi(v' = 6, J' = 24)$ transition of NaRb corresponds to the 632.8 nm-wavelength of a HeNe laser, we choose to implement this scheme using NaRb. A high-resolution monochromator is used here with its slits opened wide in order to mimic the resolution of an interference filter. Finally, the spatial dependence of the fringe field of a parallel plate capacitor is probed using a movable iris (see figure 2). This experimental setup is described in detail in the next section. Section 3 gives a model of the field dependence of the fluorescence signal. This model is used to predict the field-dependent fluorescence image surrounding a parallel plate capacitor and compared to experiment in section 4. Conclusions are left to section 5.

2. Experimental details

NaRb contained in an alkali-resistant glass cell is placed in an oven and heated to produce a vapour pressure of approximately 10^{-3} Torr. Two stainless steel disc-shaped plates of diameter 6.5 mm are placed inside the cell to form a parallel-plate capacitor of gap 1.0 mm. The plates are supported by electrodes that feed through the glass cell so that they may be biased by a variable dc power supply. The 632.8 nm output of a HeNe laser is used to excite the X $^1\Sigma^+$ (electronic ground) state ^{23}Na^{87}Rb with $v'' = 10$ quanta of vibration and $J'' = 24$ quanta of rotation via a Q-branch transition to the B $^1\Pi$ state with $v' = 6$ quanta of vibration and $J' = 24$ quanta of rotation. The 594.4 nm fluorescence produced as this excited NaRb decays to the $v'' = 0$, $J'' = 23$, 24 and 25 levels of the X $^1\Sigma^+$ state is measured as a function of both the location of the fluorescence and its polarization. The observed fluorescence is collected through a monochromator configured with wide slits. In this configuration, the band pass of the monochromator is 0.5 nm. This bandwidth is narrow enough to eliminate scattered light, but too broad to completely discriminate between the R-, P-, and Q-branch fluorescence. The monochromator is used because of its availability to the laboratory. It could easily be replaced by an interference filter. Such a setup would allow for direct imaging of the emitted fluorescence.

3. Theory of measurement

The theory of fluorescence of a $^1\Pi$ state in an electric field is covered in detail [5, 6] whereas the fundamental physics of this problem is covered in many sources [7]. Here we review the fundamental principles of this theory in the context of the NaRb system. Specifically, we consider the interaction of the Λ-doublet components of a $^1\Pi(v', J')$-state molecule produced by laser excitation of a $^1\Sigma^+(v'', J'')$ state. In the presence of an electric field, we excite a coherent superposition of both Λ-doublet components of the $^1\Pi(v', J')$ state. This superposition of excited states produces fluorescence with a polarization that is dependent on the degree of field-dependent mixing. In our model we assume that the electric field is not so strong that it dramatically alters the ground state and that the bandwidth of the excitation laser is much broader than the Stark shift of the energy levels.

3.1. Distortion of the electronic wavefunctions by a static electric field

We begin by considering the effect of an applied static field on the molecular wavefunctions. In the absence of an electric field the wavefunction of a rotating diatomic molecule in a $^1\Pi$ state is given by

$$|J'M'\,{}^1\Pi_{e/f}\rangle = |J'M'\,{}^1\Pi_{\varepsilon}\rangle = \frac{[|J'M'\Lambda\rangle|\Lambda\rangle + \epsilon|J'M' - \Lambda\rangle|-\Lambda\rangle}{\sqrt{2}}. \quad (1)$$

Here $|\Lambda\rangle$ is the electronic wavefunction for the projection of the electronic orbital angular momentum on the molecular axis. The wavefunction $|J'M'\Lambda\rangle$ describes the overall rotation of the molecule. The eigenvalue of the electronic parity operator is

given by $\epsilon = \pm 1$ and the overall parity of the molecule is given by $P_\Pi = \epsilon(-1)^{J'}$. Conventional notation [8] dictates that Λ-doublet levels with $\epsilon = +1$ are labelled e whereas Λ-doublet states with $\epsilon = -1$ are labelled f. At high J' the electronic wavefunction is symmetric with respect to reflection through any plane containing the rotation axis of the molecule for the $e(\epsilon = +1)$ levels and antisymmetric for the $f(\epsilon = -1)$ levels [9–11].

Because the electric field $\mathcal{E}$ destroys the spherical symmetry of the system, neither the rotational quantum number J nor the parity quantum number ε are good quantum numbers of the eigenstate. The cylindrical symmetry is not, however, destroyed by the external electric field. For this reason, the projection quantum numbers of the ground-state angular momenta μ and excited state angular momenta M remain conserved. Unless the applied electric field is very strong, it is still useful to label the distorted eigenstates with J and ε. We write the distorted wavefunction of the $^1\Pi$ state as

$$|M\,{}^1\Pi;\, J'\varepsilon\rangle = \sum_{J_s'=1}^{\infty} \sum_{\varepsilon_s=\pm 1} C_{\Pi M}^{J'k}(J_s', \varepsilon_s)|J_s' M\,{}^1\Pi_{\varepsilon_s}\rangle. \tag{2}$$

Of course the index $\varepsilon = \pm 1$ is no longer the eigenvalue of the electronic parity operator and J' is no longer the quantum number of the total angular momentum operator. Instead $|M\,{}^1\Pi;\, J'\varepsilon\rangle$ denotes the state that evolves adiabatically from the field-free state $|J'M'\,{}^1\Pi_\varepsilon\rangle$ as the electric field is slowly increased from zero. Here the coefficients $C_{\Pi M}^{J'k}(J_s', \varepsilon)$ give the static-field mixing of the field-free wavefunctions of given values of M, Λ-doublet state ε_s, and angular momentum J_s'. Thus, at zero field, we have

$$C_{\Pi M}^{J'\varepsilon}(J_s', \varepsilon_s) = \delta_{\varepsilon\varepsilon_s}\delta_{JJ_s'} \qquad \text{for } \mathcal{E} = 0. \tag{3}$$

For the ground $^1\Sigma^+$ state in the absence of an electric field, the wavefunction may be represented by $|J''\mu\,{}^1\Sigma^+\rangle$ where J'' gives the total angular momentum quantum and μ the projection angular momentum quantum number. As the field is turned on, these J''–μ'' states evolve into states $|\mu''\,{}^1\Sigma^+;\, J''\rangle$ where

$$|\mu''\,{}^1\Sigma^+;\, J''\rangle = \sum_{J_s''=0}^{\infty} C_{\Sigma\mu''}^{J''}(J_s'')|J_s''\mu''\,{}^1\Sigma\rangle. \tag{4}$$

The coefficients $C_{\Pi M}^{J'\varepsilon}(J_s', \varepsilon_s)$ and $C_{\Sigma\mu''}^{J''}(J_s'')$ are found from diagonalization of the Hamiltonian accounting for both molecular rotation and the Stark effect.

3.2. General expression for the polarization-dependent intensity of the laser-induced fluorescence

Using a general density matrix approach [11, 12–14], one may write the density matrix element ${}^{\varepsilon\varepsilon'}\rho_{MM'}$ of the electronic excited state as

$${}^{\varepsilon\varepsilon'}\rho_{MM'} = \frac{\hbar\tilde{\Gamma}_p}{\hbar\Gamma + \mathrm{i}\,{}^{\varepsilon\varepsilon'}\Delta_{MM'}} \sum_{\mu''} \langle M\,{}^1\Pi;\, J'\varepsilon|\hat{\boldsymbol{E}}^* \cdot \hat{\boldsymbol{D}}|\mu''\,{}^1\Sigma;\, J''\rangle \times \langle \mu''\,{}^1\Sigma;\, J''|\hat{\boldsymbol{E}} \cdot \hat{\boldsymbol{D}}^*|M'\,{}^1\Pi;\, J'\varepsilon'\rangle. \tag{5}$$

Here the summation over μ'' is over the magnetic sublevels of the ground state $^1\Sigma$ with rotational quantum number J'' whereas M and M' are magnetic sublevels of the excited state with rotational quantum number J', belonging to Λ-doublet components $\varepsilon = \pm 1$ and $\varepsilon' = \pm 1$. The unit vector $\hat{\boldsymbol{E}}$ describes the polarization of exciting laser beam, $\hat{\boldsymbol{D}}$ is a transition dipole moment unit vector, $\tilde{\Gamma}_p$ is the reduced absorption rate, Γ is the effective excited state relaxation rate, and ${}^{\varepsilon\varepsilon'}\Delta_{MM'}$ is energy splitting between the $|M'\,{}^1\Pi;\, J'\varepsilon'\rangle$ and $|M\,{}^1\Pi;\, J'\varepsilon\rangle$ states. The excited state density matrix ${}^{\varepsilon\varepsilon'}\rho_{MM'}$ allows one to calculate the intensity of the fluorescence $I_f(\hat{\boldsymbol{E}}_f)$ originating from this state in the transition $^1\Pi(v', J') \rightarrow {}^1\Sigma(v, J)$ and possessing polarization $\hat{\boldsymbol{E}}_f$:

$$I_f(\hat{\boldsymbol{E}}_f) = \tfrac{1}{4} I_0 \sum_{\varepsilon,\varepsilon',M,M',\mu} \langle M\,{}^1\Pi;\, J'\varepsilon|\hat{\boldsymbol{E}}_f^* \cdot \hat{\boldsymbol{D}}_f|\mu\,{}^1\Sigma;\, J\rangle \times \langle \mu\,{}^1\Sigma;\, J|\hat{\boldsymbol{E}}_f \cdot \hat{\boldsymbol{D}}_f^*|M'\,{}^1\Pi;\, J'\varepsilon'\rangle\,{}^{\varepsilon\varepsilon'}\rho_{M'M}. \tag{6}$$

Here I_0 is a proportionality coefficient and $\hat{\boldsymbol{D}}_f$ refers to the transition dipole unit vector for the spontaneous emission.

To evaluate $I_f(\hat{\boldsymbol{E}}_f)$, each of the dipole matrix elements are rewritten in terms of the field-free wavefunctions using the expansions of equations (2) and (4). For example the matrix element $\langle M\,{}^1\Pi;\, J'\varepsilon|\hat{\boldsymbol{E}}^* \cdot \hat{\boldsymbol{D}}|\mu''\,{}^1\Sigma;\, J''\rangle$ appearing in the excited state density matrix is written as

$$\langle M\,{}^1\Pi;\, J'\varepsilon|\hat{\boldsymbol{E}}^* \cdot \hat{\boldsymbol{D}}|\mu''{}^1\Sigma;\, J''\rangle = \sum_{J_s''J_s'\varepsilon_s} C_{\Pi M}^{J'\varepsilon}(J_s', \varepsilon_s) C_{\Sigma\mu}^{J''}(J_s'') \langle J_s' M\,{}^1\Pi_\varepsilon|\hat{\boldsymbol{E}}^*\hat{\boldsymbol{D}}|J_s''\mu''\,{}^1\Sigma\rangle. \tag{7}$$

This expression for the matrix element in terms of field-free wavefunctions allows us to take advantage of the Wigner–Eckart theorem [11, 12, 15–17]. The matrix element appearing in the summation of equation (7) becomes

$$\langle J_s' M\,{}^1\Pi_{\varepsilon_s}|\hat{\boldsymbol{E}}^*\hat{\boldsymbol{D}}|J_s''\mu''\,{}^1\Sigma\rangle = \sum_k E^{k*}(-1)^{J_s'-M} \begin{pmatrix} J_s' & 1 & J_s'' \\ -M & k & \mu'' \end{pmatrix} \langle J_s', \varepsilon_s\|\hat{\boldsymbol{D}}\|J_s''\rangle. \tag{8}$$

Here the term in large parentheses is the three-j symbol, and $\langle J_s', \varepsilon_s|D|J_s''\rangle$ is the reduced matrix element [12, 18] and E^k are the cyclic components of the unit vector $\hat{\boldsymbol{E}}$ given by

$$E^{\pm 1} = \mp\hat{\boldsymbol{E}} \cdot \frac{(\hat{x} \pm \mathrm{i}\hat{y})}{\sqrt{2}} \qquad E^0 = \hat{\boldsymbol{E}} \cdot \hat{z}. \tag{9}$$

It follows from equations (1) and (8) that $\langle J_s', \varepsilon_s\|D\|J_s''\rangle$ is given by

$$\langle J_s', \varepsilon_s\|\hat{\boldsymbol{D}}\|J_s''\rangle = \frac{1}{\sqrt{2}}[(-1)^{J_s'+J_s''+1} + \varepsilon_s]\sqrt{G(J_s', J_s'')}. \tag{10}$$

Here $G(J_s', J_s'')$ is the Hönl–London factor with $\Lambda' = 1$ corresponding to a Π state and $\Lambda'' = 0$, corresponding to the Σ state:

$$G(J_s', J_s'') = (2J_s' + 1)(2J_s'' + 1) \begin{pmatrix} J_s' & 1 & J_s'' \\ -\Lambda' & \Lambda' - \Lambda'' & \Lambda'' \end{pmatrix}^2. \tag{11}$$

3.3. Assumptions

3.3.1. First assumption. We assume the electric field does not mix states with different J values. This approximation is valid because the splitting between the e–f levels is much

smaller than the splitting between rotational levels. Thus, for a large range of electric field strengths, the Λ-doublet states mix but the rotational states do not. In this range, the mixing coefficients simplify to

$$C^{\varepsilon J'}_{\Pi M}(J'_s, \varepsilon_s) = C^{\varepsilon J'}_{\Pi M}(\varepsilon_s)\delta_{J'J'_s}. \qquad C^{J''}_{\Sigma\mu}(J''_s) = \delta_{J''J''_s}. \quad (12)$$

Using this approximation, the matrix element of equation (8) becomes

$$\begin{aligned}\langle M\,^1\Pi;\, J'\varepsilon|\hat{\boldsymbol{E}}^*\cdot\hat{\boldsymbol{D}}|\mu''\,^1\Sigma;\, J''\rangle &= \sum_{\varepsilon_s=\pm1} C^{\varepsilon J'}_{\Pi M}(\varepsilon_s)\,\langle J'M\,^1\Pi_{\varepsilon_s}|\hat{\boldsymbol{E}}^*\cdot\hat{\boldsymbol{D}}|J''\mu''\,^1\Sigma\rangle \\ &= \sqrt{2}\sum_k E^{k*}(-1)^{J'-M} C^{\varepsilon J'}_{\Pi M}((-1)^{J'+J''+1}) \\ &\quad\times\begin{pmatrix} J' & J'' & 1\\ -M & \mu'' & k\end{pmatrix}\sqrt{G(J', J'')}. \end{aligned} \quad (13)$$

3.3.2. Second assumption. Provided the electric field is not too strong, the mixing coefficients can be expressed using first-order perturbation theory. The result has the elegant form given by Derouard *et al* [5]:

$$C^{\varepsilon J'}_{\Pi M}(\varepsilon) = \cos\theta_M$$

$$C^{\varepsilon J'}_{\Pi M}(-\varepsilon) = \sin\theta_M \quad (14)$$

with

$$\theta_M = \frac{1}{2}\arctan\left\{\frac{2d_p M\mathcal{E}}{\Delta^J_{ef}J'(J'+1)}\right\}. \quad (15)$$

Here Δ^J_{ef} is the field-free splitting between the e and f levels that is well approximated by the expression

$$\Delta^J_{ef} = q[J(J+1)]. \quad (16)$$

Substituting expansion terms in the form of equation (13), the excited-state density matrix ${}^{\varepsilon\varepsilon'}\rho_{MM'}$ given by equation (5) is written in terms of mixing coefficients of the form $C^{kJ'}_{M\Pi}[(-1)^{J'+J''+1}]$. These coefficients can be written as

$$\begin{aligned} C^{\varepsilon J'}_{M\Pi}((-1)^{J'+J''+1}) &= S^{J'\varepsilon J''}_M \\ &= \sin\left(\theta_M + \frac{\pi}{4}[1 - P_\Sigma(J'')P_\Pi(J', \varepsilon)]\right) \\ &= \sin\left(\theta_M + \frac{\pi}{4}(1 - [(-1)^{J''}][\varepsilon(-1)^{J'}]\right). \end{aligned} \quad (17)$$

Here $P_\Sigma(J'')$ and $P_\Pi(J', \varepsilon)$ give the parity of the ground and excited states respectively. The expression for $C^{\varepsilon J'}_{M\Pi}((-1)^{J'+J''+1})$ in terms of the sine function clearly illustrates that, in the zero-field limit ($\theta_M = 0$), the transition vanishes for the case that these two parities are equal and is unity when they are not. Thus, in the zero-field limit, the excited and ground states are coupled only by terms for which the parity changes, as is expected for an electric dipole transition.

By substituting our expression for the density matrix (equation (5)) into our expression for the field-dependent fluorescence (equation (6)) and then using expansions of the form (13) with coefficients of the form of (17), one finds an explicit expression for the field-dependent fluorescence given the approximations we have made:

$$\begin{aligned} I_f(\hat{\boldsymbol{E}}, \hat{\boldsymbol{E}}_f, \boldsymbol{\mathcal{E}}) &= (\hbar\tilde{\Gamma}_p)I_0 G(J', J)G(J', J'') \\ &\quad\times\sum_{\varepsilon,\varepsilon',M,M',\mu,\mu'',l,l',k,k'}\frac{S^{J'\varepsilon J''}_M S^{J'\varepsilon' J''}_{M'} S^{J'\varepsilon J}_M S^{J'\varepsilon' J}_{M'}}{\hbar\Gamma + \mathrm{i}\,^{\varepsilon\varepsilon'}\Delta_{MM'}} \\ &\quad\times E^{k*}E^{k'}E^{l*}_f E^{l'}_f\begin{pmatrix} J' & J'' & 1\\ -M & \mu'' & k\end{pmatrix}\begin{pmatrix} J' & J'' & 1\\ -M' & \mu'' & k'\end{pmatrix} \\ &\quad\times\begin{pmatrix} J' & J & 1\\ -M & \mu & l\end{pmatrix}\begin{pmatrix} J' & J & 1\\ -M' & \mu & l'\end{pmatrix}. \end{aligned} \quad (18)$$

3.3.3. Third assumption. To complete our model, we must determine the way in which the electric field affects the Λ-doublet splitting ${}^{kl}\Delta_{MM'} = E^{el}_{M'\varepsilon'} - E^{el}_{M\varepsilon}$. To determine this splitting, one needs Stark energy expressions $E^{el}_{M\varepsilon}$. By solving Schrödinger's equation to second order in $\mathcal{E}$ (see Mizushima *et al* [19]),

$$\begin{aligned} E^{el}_{M\varepsilon} &= \frac{1}{2}\Delta^J_{ef} + \varepsilon\sqrt{\frac{(\Delta^J_{ef})^2}{4} + \frac{d_p^2\mathcal{E}^2M^2}{[J(J+1)]^2}} \\ &\quad + \frac{d_p^2\mathcal{E}^2}{2B'_v}\left\{\frac{(J^2-1)(J^2-M^2)}{J^3(4J^2-1)}\right. \\ &\quad \left. - \frac{[(J+1)^2-1][(J+1)^2-M^2]}{(J+1)^3[4(J+1)^2-1]}\right\} + \mathrm{O}(\mathcal{E}^3). \end{aligned} \quad (19)$$

Here B'_v is the rotational constant.

Note that although we only consider the two-state mixing of Λ-doublet components of the same J, this second-order result does consider the perturbation of the energy levels by neighbouring J states. For values of electric field for which

$$|E^{JM}_\pm - E^{J\pm1M}_\mp| \ll |E^{JM}_+ - E^{JM}_-| \quad (20)$$

the second-order result given by equations (19) and (12) become invalid. As the electric field increases the number of rotational states that are significantly mixed increases as well. For fields large enough for equation (20) to be true, the applicability of our perturbation treatment breaks down and one has to solve the secular equation system [20] for the relevant Hamiltonian matrix. The analysis of such a treatment, accounting for $J \pm \Delta J$ mixing centred at initial (J''), excited (J') and final (J) rotational state of a $J'' \rightarrow J' \rightarrow J$ transition has been treated by Tamanis *et al* [6].

4. Evaluation of the polarization-dependent fluorescence

Our expression for $I_f(\hat{\boldsymbol{E}}, \hat{\boldsymbol{E}}_f)$ assumes a z-quantization axis that corresponds to the direction of the electric field. For an imaging study, the direction of the electric field is typically spatially dependent. It is therefore convenient to express the components of the electric field in a coordinate system independent way. Because of the axial symmetry of the problem, there is some freedom in the way in which this is done. For the case $\hat{\boldsymbol{E}} \neq \hat{\boldsymbol{\mathcal{E}}}$, we define the x-axis so that $\hat{\boldsymbol{E}}$ lies in the x–z-plane. For $\hat{\boldsymbol{E}} = \hat{\boldsymbol{\mathcal{E}}}$, we define the x-axis so that $\hat{\boldsymbol{E}}_f$ lies in the x–z-plane. With these choices, the x, y and z

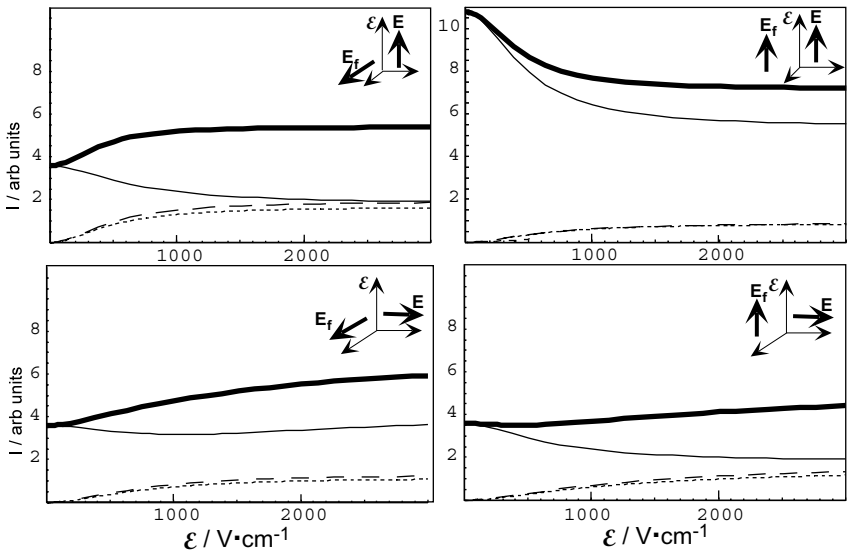

Figure 3. Expected fluorescence intensity as defined by equation (18) of the text for various orientations of the electric field $\hat{\mathcal{E}}$, laser polarization $\hat{\boldsymbol{E}}$, and fluorescence polarization $\hat{\boldsymbol{E}}_f$: thin full line, Q-branch fluorescence; short broken line, R-branch fluorescence; long broken line, P-branch fluorescence; bold line, total fluorescence.

components of $\hat{\boldsymbol{E}}$ and $\hat{\boldsymbol{E}}_f$ are given by

$$\hat{\boldsymbol{E}} = \begin{pmatrix} \sqrt{1-(\hat{\boldsymbol{E}}\cdot\hat{\boldsymbol{\mathcal{E}}})^2} \\ 0 \\ \hat{\boldsymbol{E}}\cdot\hat{\boldsymbol{\mathcal{E}}} \end{pmatrix} \tag{21}$$

$$\hat{\boldsymbol{E}}_f = \frac{1}{\sqrt{1-(\hat{\boldsymbol{E}}\cdot\hat{\boldsymbol{\mathcal{E}}})^2}} \begin{pmatrix} \hat{\boldsymbol{E}}\cdot\hat{\boldsymbol{E}}_f - (\hat{\boldsymbol{E}}_f\cdot\hat{\boldsymbol{\mathcal{E}}})(\hat{\boldsymbol{E}}\cdot\hat{\boldsymbol{\mathcal{E}}}) \\ (\hat{\boldsymbol{E}}\times\hat{\boldsymbol{\mathcal{E}}})\cdot\hat{\boldsymbol{E}}_f \\ (\hat{\boldsymbol{E}}_f\cdot\hat{\boldsymbol{\mathcal{E}}})\sqrt{1-(\hat{\boldsymbol{E}}\cdot\hat{\boldsymbol{\mathcal{E}}})^2} \end{pmatrix}. \tag{22}$$

For $\hat{\boldsymbol{E}} = \hat{\boldsymbol{\mathcal{E}}}$,

$$\hat{\boldsymbol{E}}_f = \begin{pmatrix} \sqrt{1-(\hat{\boldsymbol{E}}_f\cdot\hat{\boldsymbol{\mathcal{E}}})^2} \\ 0 \\ \hat{\boldsymbol{E}}_f\cdot\hat{\boldsymbol{\mathcal{E}}} \end{pmatrix}. \tag{23}$$

The Cartesian components given by equations (21) and (22) can be used to evaluate the values of E^q and E_f^q defined by equation (9). By substituting these cyclic components of the laser and fluorescence radiation and using the substitutions of equations (15) and (19), one may evaluate the relative intensity $I_f(\hat{\boldsymbol{E}}, \hat{\boldsymbol{E}}_f, \vec{\mathcal{E}})$ of detected fluorescence when a $^1\Sigma$ state is excited by a laser with polarization $\hat{\boldsymbol{E}}$ and observed through a filter that allows only the polarization $\hat{\boldsymbol{E}}_f$.

Figure 3 gives the polarization- and field-dependent fluorescence expected for the cases when $\hat{\boldsymbol{E}}$ and $\hat{\boldsymbol{E}}_f$ are either perpendicular or parallel to $\vec{\mathcal{E}}$. In the present experimental arrangement, the final state is not resolved spectroscopically. For this reason, the expression for $I_f(\hat{\boldsymbol{E}}, \hat{\boldsymbol{E}}_f, \vec{\mathcal{E}})$ is summed over all possible final values of J ($J = 23$, $J = 24$, and $J = 25$). Required constants take on the values $d = 3\text{D}$ [21], $q = 2.892 \times 10^{-6}$ cm^{-1} [21], $\Gamma = 6 \times 10^7$ s^{-1} [22], and $B_v' = 0.0478$ cm^{-1} [23]. When $\hat{\boldsymbol{E}}$ and $\hat{\boldsymbol{E}}_f$ are both parallel to $\vec{\mathcal{E}}$, the expected fluorescence decreases with increasing field. For all other cases considered, the expected fluorescence increases with increasing field.

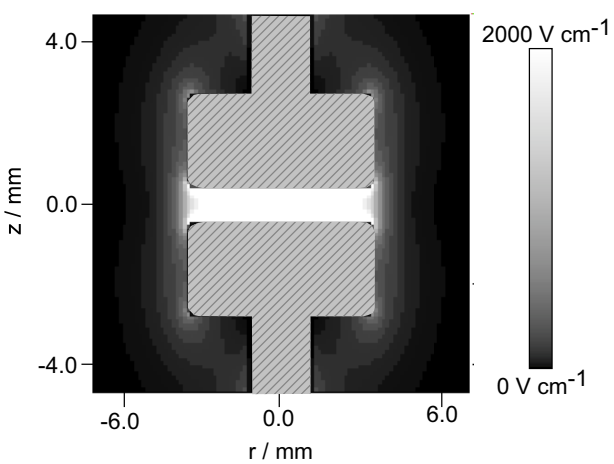

Figure 4. Magnitude of the electric field in the vicinity of the parallel-plate capacitor for the case of a 200 V potential across the terminals.

5. Experiment versus theory

Figure 4 shows the electric field between the parallel-plates of the capacitor in the experiment found using the relaxation method [24]. Figures 5 and 6 show the expected spatially-dependent LIF signal for the case that the laser polarization is parallel and perpendicular to the axis of the capacitor. The inverse relationship between fluorescence intensity and electric field strength causes a marked difference between the image of figure 5 (fluorescence polarization parallel to the capacitor axis) and figure 6 (fluorescence polarization perpendicular to the capacitor axis.)

Figures 7 and 8 compare data taken with the setup shown in figure 2 to those given by the model in equation (18). We see that the agreement between theory and experiment is only qualitative. The major source of this disagreement can be traced to our initial assumption that the bandwidth of our excitation laser is much broader than the Stark shift

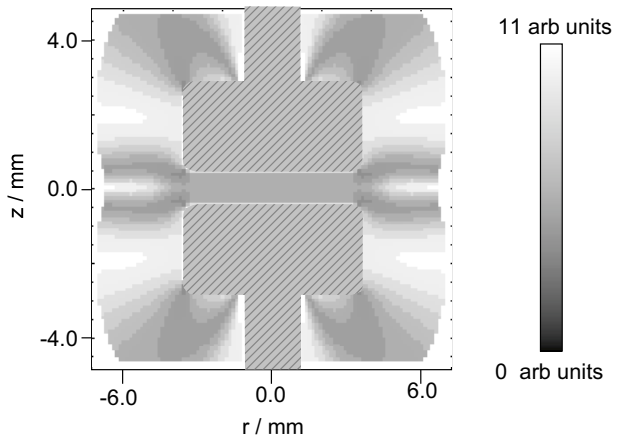

Figure 5. Expected laser-induced fluorescence image for the case of a 200 V potential across the terminals of the capacitor and laser polarization $\hat{\boldsymbol{E}}$ and fluorescence polarization $\hat{\boldsymbol{E}}_f$ directed parallel to the capacitor axis.

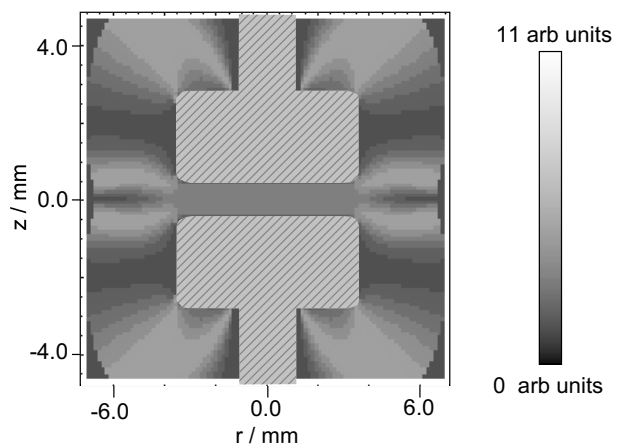

Figure 6. Expected laser-induced fluorescence image for the case of a 200 V potential across the terminals of the capacitor, laser polarization $\hat{\boldsymbol{E}}$ directed parallel to the capacitor axis, and fluorescence polarization $\hat{\boldsymbol{E}}_f$ directed perpendicular to the capacitor axis.

of the energy levels. This is only approximately true for the case of a 500 V cm^{-1} field (see figure 7). For 2000 V cm^{-1} field, the effect of the narrow bandwidth HeNe laser is more pronounced and agreement between theory and experiment becomes quite poor (figure 8). A full treatment of the effect of the bandwidth of the excitation laser will be treated in a future work.

6. Conclusion

We have found that a highly sensitive probe to an electric field in a plasma can be obtained without dispersing the fluorescence radiation. Specifically, our findings suggest the following relatively inexpensive technique for experimentally testing models of the field in a plasma: (1) introduce NaRb into the plasma; (2) use a HeNe laser to excite the NaRb; (3) use a CCD camera to image the fluorescence through a polarizer and an interference filter centered about 595 nm; (4) compare the expected fluorescence distribution to that predicted by the model field and equation (18).

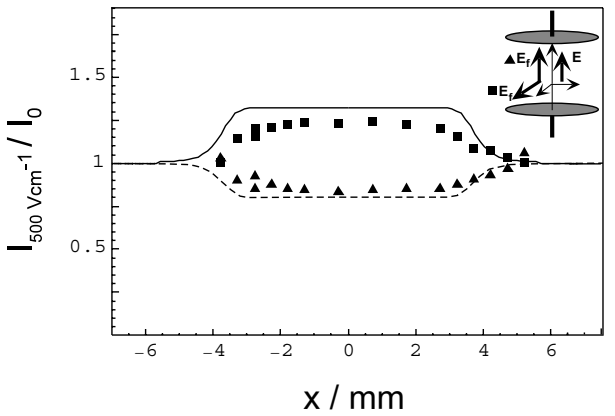

Figure 7. The ratio of fluorescence intensity for the case of a 50 V potential across the terminals to the fluorescence intensity for the case of a 0 V potential across the terminals as a function of position along an axis going through the centre of the capacitor. Here the laser polarization $\hat{\boldsymbol{E}}$ is directed parallel to the capacitor axis. Full curves and squares, comparison of prediction and experiment for $\hat{\boldsymbol{E}}_f$ directed perpendicular to the capacitor axis; broken curves and triangles, comparison of prediction and experiment for $\hat{\boldsymbol{E}}_f$ directed parallel to the capacitor axes.

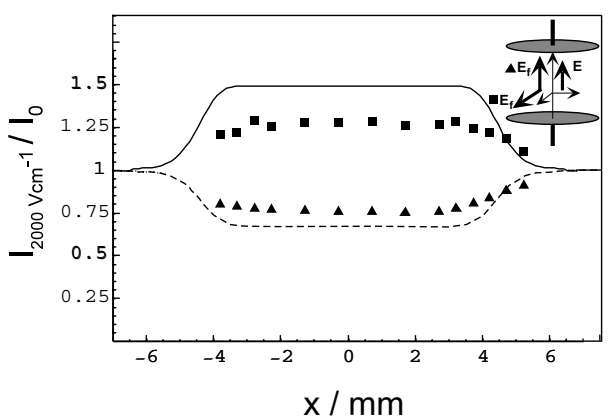

Figure 8. The ratio of fluorescence intensity for the case of a 200 V potential across the terminals to the fluorescence intensity for the case of a 0 V potential across the terminals as a function of position along an axis going through the centre of the capacitor. Here the laser polarization $\hat{\boldsymbol{E}}$ is directed parallel to the capacitor axis. Full curve and squares, comparison of prediction and experiment for $\hat{\boldsymbol{E}}_f$ directed perpendicular to the capacitor axes; broken curve and triangles, comparison of prediction and experiment for $\hat{\boldsymbol{E}}_f$ directed parallel to the capacitor axis.

Whereas agreement between our model and theory is currently qualitative, we have clearly demonstrated that the effect of Λ-doublet mixing on the polarization of the $^1\Sigma(v'', J'') \rightarrow {}^1\Pi(v', J') \rightarrow {}^1\Sigma(v, J)$ laser-induced-fluorescence scheme provides a sensitive probe of an electric field in a plasma.

Acknowledgments

We are thankful to I Klincare and O Hrabrova for assistance in the preparation of the experiment. We gratefully acknowledge financial support by the Ministry of Education and Science

of Latvia in the form of a grant to support market-oriented research. This work is also supported by the National Research Council (NRC-6224) and the National Science Foundation (CHE-9875456).

References

[1] Lawler J and Doughty D 1994 *Adv. At. Mol. Opt. Phys* **34** 171
[2] Moore C A, Davis G P and Gottscho R A 1984 *Phys. Rev. Lett.* **52** 538
[3] Derouard J and Sadeghi H 1986 *Opt. Commun.* **57** 239
[4] Derouard J, Debontride H, Nguyen T D and Sadeghi N 1989 *J. Chem. Phys.* **90** 5936
[5] Derouard J and Alexander M H 1986 *J. Chem. Phys.* **85** 134
[6] Tamanis M *et al* 1997 *J. Chem. Phys.* **106** 2195
[7] Shore B 1990 *The Theory of Coherent Atomic Excitation* (New York: Wiley) pp 209–15
[8] Brown J *et al* 1975 *J. Mol. Spectrosc.* **55** 500
[9] Alexander M and Dagdigian P 1984 *J. Chem. Phys.* **80** 4325
[10] Townes C H and Schawlow A L 1975 *Microwave Spectroscopy* (Dover, UK: Dover Publications)
[11] Blum K 1996 *Density Matrix Theory and Application* (New York: Plenum)
[12] Auzinsh M and Ferber R 1995 *Optical Polarization of Molecules* (Cambridge: Cambridge University Press) pp 12–306
[13] Cohen-Tannoudji C 1962 *Ann. Phys.* **7** 423
[14] Cohen-Tannoudji C 1962 *Ann. Phys.* **7** 469
[15] Zare R 1988 *Angular Momentum, Understanding Spatial Aspects in Chemistry and Physics* (New York: Wiley–Interscience) pp 15–349
[16] Sobelman I I 1992 *Atomic Spectra and Radiative Transitions* (Berlin: Springer) pp 16–356
[17] Edmonds A R 1974 *Angular Momentum in Quantum Mechanics* (Princeton, NJ: Princeton University Press) pp 17–146
[18] Varshalovich V D A and Moskalev A N 1988 *Quantum Theory of Angular Momentum* (Singapore: World Scientific) pp 18–514
[19] Mizushima M 1975 *Theory of Rotating Diatomic Molecules* (New York: Wiley) pp 19–543
[20] Roegger 1971 *J. Phys. B: At. Mol. Phys.* **4** 188
[21] Nikolayeva O *et al* 2000 *J. Chem. Phys.* **113** at press
[22] Kasahara S *et al* 1996 *J. Chem. Phys.* **105** 1341
[23] Wang Y-C *et al* 1991 *J. Chem. Phys.* **95** 6229
[24] Press W, Flannery B, Teukolsky S and Vetterling W 1986 *Numerical Recipes* (Cambridge: Cambridge University Press) pp 24–818